HHS Public Access

Author manuscript

Magn Reson Med. Author manuscript; available in PMC 2023 February 01.

Published in final edited form as:

Magn Reson Med. 2022 February ; 87(2): 629–645. doi:10.1002/mrm.28991.

Comparison of prospective and retrospective motion correction in 3D-encoded neuroanatomical MRI

Jakob M. Slipsager[1,2,3,4], **Stefan L. Glimberg**[3], **Liselotte Højgaard**[2], **Rasmus R. Paulsen**[1], **Paul Wighton**[4], **M. Dylan Tisdall**[5], **Camilo Jaimes**[6,7], **Borjan A. Gagoski**[7,8], **P. Ellen Grant**[7,8], **André van der Kouwe**[4,7], **Oline V. Olesen**[1,2,3], **Robert Frost**[4,7]

[1]DTU Compute, Technical University of Denmark, Denmark

[2]Dept. of Clinical Physiology, Nuclear Medicine & PET, Rigshospitalet, University of Copenhagen, Denmark

[3]TracInnovations, Ballerup, Denmark

[4]Athinoula A. Martinos Center for Biomedical Imaging, Massachusetts General Hospital, Charlestown, Massachusetts

[5]Department of Radiology, Perelman School of Medicine, University of Pennsylvania, Philadelphia, Pennsylvania

[6]Boston Children's Hospital, Boston, Massachusetts

[7]Dept. of Radiology, Harvard Medical School, Boston, Massachusetts

[8]Fetal-Neonatal Neuroimaging & Developmental Science Center, Boston Children's Hospital, Boston, Massachusetts

Abstract

Purpose—To compare prospective motion correction (PMC) and retrospective motion correction (RMC) in Cartesian 3D-encoded MPRAGE scans and to investigate the effects of correction frequency and parallel imaging on the performance of RMC.

Methods—Head motion was estimated using a markerless tracking system and sent to a modified MPRAGE sequence which can continuously update the imaging FOV to perform PMC. The prospective correction was applied either before each echo-train (Before-ET) or at every sixth readout within the echo-train (Within-ET). RMC was achieved by adjusting k-space trajectories according to the measured motion during image reconstruction. The motion correction frequency was retrospectively decreased or increased through RMC or reverse RMC. Phantom and in vivo experiments were used to compare PMC and RMC, and to compare Within-ET and Before-ET correction frequency during continuous motion. The correction quality was quantitatively evaluated using the structural similarity index measure using a reference image without motion correction and without intentional motion.

Contact information corresponding author: Jakob M. Slipsager, DTU Compute, Technical University of Denmark, Building 324, Richard Petersens Plads, DK-2800 Kgs. Lyngby, Denmark, jmsl@dtu.dk.

Results—PMC resulted in superior image quality compared to RMC both visually and quantitatively. Increasing the correction frequency from Before-ET to Within-ET reduced motion artifacts in RMC. A hybrid PMC and RMC correction, i.e. retrospectively increasing the correction frequency of Before-ET PMC to Within-ET also reduced motion artifacts. Inferior performance of RMC compared to PMC was shown with GRAPPA calibration data without intentional motion, and without any GRAPPA acceleration.

Conclusion—Reductions in local Nyquist violations with PMC resulted in superior image quality compared to RMC. Increasing the motion correction frequency to Within-ET reduced motion artifacts in both RMC and PMC.

Introduction

Head motion is an ongoing problem in MR imaging of the brain, causing artifacts that reduce clinical image quality and introduce bias and variance in research results [1,2]. In the clinic, sequences may be repeated to ensure images with sufficient quality are obtained for diagnostic use, but at the expense of prolonged examination times and increased financial cost. Andre et al. [3] showed that in 19.8% of the MRI examinations they studied it was necessary to repeat at least one of the sequences, adding an estimated extra cost of $115,000 per scanner per year. In pediatric MRI examinations, sedation or anesthesia are commonly used to mitigate motion, but these methods are associated with increased health risk and additional costs [4,5]. In a recent study the estimated annual cost of pediatric anesthesia in MRI examinations was $319,000 per scanner [6].

To reduce the negative effects of head motion, several motion correction (MC) strategies have been proposed. Overall, MC techniques can be divided into either prospective motion correction (PMC) or retrospective motion correction (RMC).

In PMC, the correction is performed by modifying the acquisition as data is acquired. This requires continuous, low latency estimation of the rigid body position and orientation (pose) of the patient's head throughout the scan. These estimates are used to dynamically adjust the encoding field-of-view (FOV) to keep it stationary relative to the patient's head [7,8]. The different approaches to estimate head motion can be divided into MR-based "navigator" techniques, and external systems that require some additional hardware. Navigators are sequence modules embedded in the parent sequence that acquire additional data for motion estimation, and with some common methods a new motion estimate is provided every few seconds [9–13]. There are also various self-navigated approaches that estimate head motion directly from the acquired imaging data [14–18]. In contrast, external tracking systems use additional hardware, either MR or optical (e.g. cameras, light sources, and markers) to estimate motion at a temporal scale in the millisecond range [19–26].

RMC covers a large group of strategies, where the correction of motion takes place after the data acquisition is complete. Methods working in the k-space domain, use the estimated motion to update the k-space trajectory in the image reconstruction [12,27]. The k-space trajectory can also be updated without explicitly measuring the motion. Early methods iteratively corrected the acquired data to optimize image quality measures (e.g. entropy

or gradient entropy) [28,29]. Recent methods estimate motion from the data itself using the motion information encoded in the multiple receiver coils [15,16].

Some of the advantages of RMC are that it preserves the original uncorrected image and it is not dependent on receiving real-time motion measurements with low latency. However, RMC is less effective in 2D multi-slice segmented sequences when there is through-slice motion between segments [30]. 3D-encoded acquisitions also suffer from k-space under-sampling in the presence of head rotations[8] which lead to violation of the Nyquist criterion and cannot be compensated by RMC using the non-uniform Fourier transform to reconstruct the irregularly-sampled k-space. In principle, prospective correction of the acquisition will sample k-space as intended and thereby avoid such gaps in k-space. For this reason, PMC is expected to be less susceptible to under-sampling artifacts, although to date, this has not been shown empirically.

In the context of recent developments for RMC in 3D-encoded MRI [12,17,18,31], the first aim of this work was to compare the motion correction performance of PMC and RMC in 3D-encoded structural MRI of the brain. Previously, navigator and optical tracking modalities have been compared for retrospective correction of involuntary motion in high-resolution structural sequences [32]. Also, prospective correction with NMR field probes versus optical tracking [33] has been compared. In this study, we directly compare retrospective and prospective correction in Cartesian 3D-encoded MPRAGE with the same markerless optical tracking [25,26,34].

The second aim was to investigate the effect of the correction frequency on the encoding error and the performance of RMC. Increasing the correction frequency of PMC in 3D MPRAGE has previously been shown to reduce image artifacts [26]. RMC was used to retrospectively increase and decrease the correction frequency of the acquired data.

Finally, experiments were performed to investigate the effects of GRAPPA calibration and reconstruction in comparisons between PMC and RMC. Parallel imaging is routinely used to accelerate 3D-encoded MRI acquisitions. However, differences in performance between RMC and PMC could be due to motion-related effects on the calibration and parallel imaging reconstruction. The use of GRAPPA auto-calibration signal (ACS) data without intentional motion from a pre-scan was compared with integrated ACS. Furthermore, comparisons of PMC and RMC were performed without any GRAPPA acceleration – this removes the GRAPPA confound in performance comparisons and leaves only the effect of k-space undersampling due to rotation.

Methods

Motion tracking

Rigid-body head motion was estimated using a 2nd generation of the markerless tracking system [35] Tracoline TCL3.1 (TracInnovations, Ballerup, Denmark) [25,26]. The TCL3 system was placed behind the scanner and the vision probe containing the non-electronic system optics was attached to the scanner table. The probe was positioned to have an unobstructed line of sight to the subject's face through the 64-channel head coil (Siemens Healthineers,

Erlangen, Germany). The TCL3 system estimates motion by capturing 3D surface scans of the subject's face at a rate of 30 Hz using near-infrared structured light. Head motion is estimated by computing the rigid body transformation that maps the current surface scan back to the initial reference surface. TCL3 uses an iterative closest point algorithm to estimate the rigid body transformation between the surface scans [35].

A geometric calibration between the scanner and the TCL3 system is necessary to represent the estimated motion in the coordinate system of the scanner. For retrospective correction, a temporal calibration is also required. The geometric alignment consists of a cross-calibration where the reference surface scan of the subject is matched to a surface extracted from a structural MRI calibration scan [36]. The subjects were asked to remain still during the cross-calibration scan and this was verified with the tracking. The cross-calibration results in a transformation ${}_{scs}\mathbf{A}_{tcs}$ between the scanner coordinate system (scs) and the TCL3 coordinate system (tcs).

The temporal calibration was achieved by a time synchronization between the TCL3 computer and the host computer of the scanner. Both calibration steps were performed before each scan session.

Prospective motion correction

PMC was enabled by modifying a Cartesian 3D-encoded MPRAGE sequence to adjust the imaging field of view (FOV) according to motion estimates received from the TCL3 system [26]. To examine the effect of the update frequency on the correction performance, two different versions of the PMC MPRAGE sequences were tested [26]. In the first version, referred to as Before-ET-PMC, the FOV was updated before each ET, with ETs 2500 ms apart. In the second version, referred to as Within-ET-PMC, the FOV was updated before each ET and every six readouts (48 ms update interval) within the ET.

Retrospective motion correction

RMC was performed on an external computer using a modified version of the freely available retroMoCoBox software package [37] and consists of the following steps:

1. Reconstruction of missing k-space lines due to GRAPPA acceleration [38].
2. Each k-space readout is temporally matched to the nearest available motion estimate recorded by the tracking device. As a result, each readout is then assigned a 4x4 homogeneous transformation matrix ${}_{tcs}\mathbf{T}_{tcs}(e,r)$. The transformation matrix encodes the head pose of the subject at the r'th readout in the e'th ET relative to a reference position of the subject.
3. The assigned motion is transformed into scanner's coordinate system (*scs*) using the cross-calibration ${}_{scs}\mathbf{T}_{scs}\left(e,r\right) = {}_{scs}\mathbf{A}_{tcs}\,{}_{tcs}\mathbf{T}_{tcs}\left(e,r\right)\,{}_{scs}\mathbf{A}_{tcs}^{-1}$.
4. Translations are corrected by adding additional phase ramps to each k-space readout using the assigned translation parameters.
5. Correction of rotations is done by rotating each k-space line according to the assigned rotations.

6. An implementation of the non-uniform fast Fourier transformation (NUFFT) running on the GPU [39] is used to reconstruct the image since k-space is no longer uniformly sampled as a result of the k-space trajectory correction.

RMC was also applied to data acquired with Before-ET-PMC to retrospectively increase the motion correction frequency during echo-trains. This hybrid motion correction (HMC) strategy could be termed Within-ET-HMC. This was done by passing the raw data from the Before-ET-PMC scan through the RMC pipeline to correct for residual motion that occurred when the subject moved during an echo-train (See Supporting Information Figure S 1). The residual motion $\mathbf{T}_{res}$ was determined by

$$\mathbf{T}_{res}(e,r) = \mathbf{T}^{-1}(e,0)\mathbf{T}(e,r), \tag{1}$$

where $\mathbf{T}(e,0)$ is the transformation that was used to update the FOV before the e'th ET and $\mathbf{T}(e,r)$ is a recorded transformation at the r'th readout in the e'th ET.

"Reverse" MC was performed on PMC data [27,40], to create "uncorrected" versions of both Within-ET and Before-ET PMC scans. Raw k-space data acquired with PMC were passed through the RMC pipeline. The k-space trajectory was reverse corrected with the inverted motion estimates that were used to update the FOV in real-time.

Finally, reverse motion correction was used to reconstruct Before-ET images based on Within-ET PMC data. Here, the k-space trajectory was reverse corrected by the difference between the Within-ET and the Before-ET transformations. This set of transformations were determined by

$$\mathbf{T}_{res}(e,r) = \mathbf{T}^{-1}(e,r)\mathbf{T}(e,0) \tag{2}$$

Data acquisition and reconstruction

Data in this work were acquired on a 3 T Prisma scanner (Siemens Healthineers, Erlangen, Germany) using a 64-channel head coil. All MPRAGE sequences used in the experiments had the following protocol: FOV=256x256 mm^2, matrix=256x256, 176 1 mm sagittal slices, in-plane GRAPPA R=2, TR=2500 ms, TE=3.3 ms, TI = 1070 ms, bandwidth=240 Hz/px, echo spacing=8 ms, and turbo factor=176. The scan time was 5:59 min with integrated GRAPPA ACS acquisition and 5:19 min with external ACS.

A subset of the MPRAGE scans were acquired without GRAPPA acceleration. The scan time was kept to 6:02 min by modifying the following parameters: FOV=240x225.6 mm^2, matrix=192xl80, TR=2000.

Image reconstruction

To avoid any potential differences between the reconstruction running on the scanner and the offline RMC reconstruction, all data were transferred to an external computer and reconstructed using the RMC reconstruction pipeline. For the reconstruction of PMC images, the acquired raw data were reconstructed with the RMC pipeline, but the k-space trajectory was updated with the identity matrix instead of real motion estimates, as

illustrated in Figure 1A. Reconstruction of RMC and uncorrected images is illustrated in Figure 1B. Here the k-space trajectory was updated either with motion estimates recorded during the scan for RMC images, or with the identity matrix for uncorrected images.

GRAPPA calibration and reconstruction

The relevance of GRAPPA to the comparison of PMC and RMC is that commonly-used RMC based on Gallichan et al. [12] estimates the GRAPPA weights and reconstructs missing k-space data before any motion correction. The auto-calibration signal (ACS) data [38] for GRAPPA-accelerated MPRAGE is typically integrated into the acquisition by fully sampling central k-space lines, but alternatively, can be acquired in an external FLASH pre-scan. Hence, with integrated ACS acquisition, motion during the ACS region is expected to corrupt both the estimation of GRAPPA weights and the reconstruction of missing k-space data. Alternatively, if we arrange an “ideal” external ACS acquisition without intentional motion, the GRAPPA weights can be estimated accurately, but we expect that the reconstruction of missing k-space still suffers from applying a “correct” GRAPPA kernel to irregularly sampled k-space lines that are phase-shifted or rotated by rigid motion.

RMC using the external ACS option was compared with using integrated ACS. The integrated ACS images have higher signal-to-noise ratio than external ACS images, because the extra ACS k-space data are used in the reconstruction instead of estimated. Hence, for controlled comparisons with external ACS images, the integrated ACS k-space lines were not used in the reconstructed images, i.e., they were only used to calculate the GRAPPA weights.

To remove the confound of GRAPPA in the comparison of PMC and RMC, experiments without GRAPPA acceleration were also performed.

Experiments

Phantom and in vivo experiments were performed to investigate the correction performance of PMC and RMC and to assess the effect of correction frequency on the performance during continuous motion. A summary of the performed experiments is given in Table 1. As a gold standard for the image quality, an uncorrected reference scan without intentional motion was acquired for every subject.

The in vivo experiments were performed on six healthy volunteers, who were scanned in accordance with Institutional Review Board guidelines. Before each scan session, the volunteers were trained to move their heads in a repeatable pattern in order to obtain PMC data and uncorrected data (for RMC) corrupted by similar motion. Subjects did not have head padding so they could move and maintain a head pose without having to strain against the padding. Similar motion across compared scans could be qualitatively confirmed from motion plots on the TCL3 display. MPRAGE scans using Within-ET PMC and no MC (for RMC) were carried out for every subject.

Comparison of PMC and RMC in vivo experiments

In session one, the performed pattern was discrete, abrupt motion, where the volunteer changed head position (look right, up, left, down, back to center) at 1-minute intervals.

In scan session two, the performed pattern was periodic, continuous motion. Here, for a 1-minute period that started 2 minutes into the sequence the volunteer continuously changed head position by looking left to right.

In session one and two, the pattern was performed with a medium and high motion amplitude. The maximum amplitude of deviation in scanner coordinates from the starting positions were: ~2.5 mm and ~5° for medium discrete motion; ~5 mm and ~10° for large discrete motion; ~1.5 mm and ~3° for medium continuous motion; ~2.5 mm and ~5° for large continuous motion. Motion plots are provided along with each image comparison.

In session three, both the discrete and periodic continuous motion patterns were tested in separate scans.

Motion correction frequency phantom experiments

A pineapple was placed in a mechanical device that was able to rotate the pineapple around the scanner's vertical y-axis. The pineapple was continuously moved back and forth for 1 minute with maximum amplitude of deviation in scanner coordinates from the starting positions of ~5 mm and ~3.5°. This motion was reproduced as consistently as possible during MPRAGE scans with no MC, Before-ET PMC, and Within-ET PMC. This procedure was performed for three motion onset times, with the motion period beginning at approximately 0, 1, and 2 minutes into the MPRAGE scans (see Supporting Information Figure S 2). The recorded motion for the 2 minute motion onset time is shown in Figure 5 in the coordinate system of the scanner.

Motion correction frequency in vivo experiments

Scan session two was designed to investigate the effect of update frequency on motion correction performance and thus, Before-ET PMC scans were also acquired in session two.

GRAPPA calibration in vivo experiments

Scan sessions four and five investigated the effect of using integrated versus external acquired GRAPPA calibration data on the quality of RMC during discrete and continuous motion. The volunteers did not move intentionally during the external ACS acquisitions at the start of the scan.

In vivo experiments without GRAPPA acceleration

In scan session six the potential confounds related to GRAPPA were removed by comparing PMC and RMC in un-accelerated acquisitions, leaving only effects related to k-space undersampling. Discrete and continuous motion patterns were tested.

Quantification of motion

Image encoding errors were quantified by calculating the discrepancy between the encoded FOV and the estimated true FOV (based on the pose from the motion tracker) at each k-space readout[26]. At each readout r in each ET e, the true and the encoded positions can be described by a 4x4 transformation matrix $\mathbf{T}_{true}(e,r)$ and $\mathbf{T}_{encode}(e,r)$, respectively. The discrepancy $d(e,r)$ between encoded and true positions was determined as the average voxel displacement deviation over a 64 mm-radius sphere[41]. The discrepancy over the entire sequence is quantified as the RMS discrepancy by

$$RMS_{discrepancy} = \sqrt{\frac{1}{ER}\sum_{e=1}^{E}\sum_{r=1}^{R} d(e,r)^2}, \quad (3)$$

where R is the number of readouts in an ET and E is the number of ETs.

The head motion in each scan was also quantified using the RMS discrepancy. The discrepancy $d(e,r)$ was calculated between the recorded $\mathbf{T}recorded(e,r)$ motion and the identity matrix.

Quantification of image quality

Image quality was quantified relative to an uncorrected image without intentional motion (reference image) recorded in each scan session. Rigid registration with the Insight Toolkit [42,43] was performed on each image volume within a session using the reference image as the fixed volume. The background of each volume was removed by a mask created from the reference image. The structural similarity index measure (SSIM) [44] between the foreground of the evaluated image and the reference image was used as a measure of the image quality.

Results

Image quality comparison of prospective and retrospective correction

Comparisons of image quality during discrete and continuous head motion are shown in Figure 2 and Figure 3 respectively, together with the recorded head motion. Results from scan session 3 are shown in Supporting Information Figure S 3. Both PMC and RMC provide improved image quality compared to the uncorrected scans. A direct comparison of the images in the medium amplitude discrete motion cases in Figure 2B shows that the PMC image is marginally better than the RMC image which is more blurred and has less contrast. However, in the case of large discrete motion (Figure 2B and Supporting Information Figure S 3B), the PMC image quality is substantially better than for the corresponding RMC images. In the periodic continuous motion experiments (Figure 3B and Supporting Information Figure S 3B) more artifacts are evident in RMC than in the PMC images. The three volunteers were able to repeat similar motion patterns in nearly all scans. However, in the case of large discrete (subject 1) and continuous (subject 3) motion, there is lower motion amplitude during the PMC scans than in the uncorrected scans used for RMC.

The magnitude of k-space data after no MC, PMC, and RMC during high amplitude discrete and continuous motion are shown in Supporting Information Figure S 4 demonstrating that

k-space after RMC contains under- and over-sampled regions. This effect is seen from both types of motion pattern, but it is most notable in the discrete motion case.

Figure 4 shows the image quality as measured by SSIM plotted as a function of the RMS discrepancy during the corresponding motion. The image quality is reduced (lower SSIM) when the motion increases in nearly every case. It is also seen that both PMC and RMC results in higher SSIM compared to the uncorrected images, however, PMC results in the highest SSIM in every case. In the scan corrupted by large continuous motion (subject 2), RMC resulted in a slightly lower SSIM compared to the uncorrected image, despite a visual improvement in sharpness and contrast (see Figure 3B, bottom row).

Effect of FOV correction frequency on RMC image quality.

The recorded motion estimates and images from the phantom experiments with motion onset at 0, 1, and 2 minutes into the sequence are shown in Supporting Information Figure S 2. Images acquired during motion starting 2 minutes into the sequences are shown in Figure 5A. Images along the diagonal were acquired with PMC off, Before-ET PMC, and Within-ET PMC and reconstructed without RMC. Images outside the diagonal are retrospectively corrected or reverse corrected versions of the images in the diagonal. Thus, there are three reconstructed images for each acquired scan. Both RMC and PMC before each ET increase image quality (column 2, rows 1 and 2). Increasing the update rate to Within-ET MC results in even better image quality for data acquired with PMC off and Before-ET PMC, as seen from rows 1 and 2 in column 3. Retrospectively updating the Before-ET PMC scan to Within-ET correction resulted in similar quality to the native Within-ET PMC scan (column 3, rows 2 and 3). The same retrospective correction and reverse correction schemes were applied to the phantom experiments with motion starting 0 and 1 minute into the sequences. These experiments show similar results to the experiment with motion starting at 2 minutes, but with fewer motion artifacts in the uncorrected images and therefore less-notable effects of MC were seen.

The same retrospective correction scheme was applied to the in vivo experiments with periodic continuous motion (subject 2). The recorded motion and reconstructed images are shown in Figure 6 for the high motion amplitude experiment, where each row corresponds to a scan. The in vivo experiments show similar results as the phantom experiments, where Within-ET correction (both PMC and RMC) provides images with the best quality. However, in the in vivo experiments the best quality was provided by the PMC, while RMC resulted in lower visual quality. The quality of the combined PMC and RMC falls between the PMC and RMC.

In both the phantom and in vivo experiments, the discrepancy between the true motion and the encoded motion was used as a measure of the encoding error of the correction. Supporting Information Figure S 1 shows the discrepancy of rotation around the z-axis for the in vivo experiment with medium amplitude. Within-ET MC resulted in the lowest discrepancy, and Before-ET MC reduced the discrepancy compared to no MC.

In Figure 7 the SSIM is plotted as a function of the RMS discrepancy for every acquired, retrospectively corrected, and reverse corrected image. k-Space data acquired with PMC off,

Before-ET PMC, and Within-ET PMC are labeled with a blue marker. Images reconstructed from the same k-space data are connected and data points with the same color were corrupted by similar motion patterns and amplitudes. The phantom experiments (Figure 7A) show that when motion occurred early in the scan, the image quality was better than compared to scans where the motion was applied in the middle (closer to the center of k-space). Secondly, Within-ET MC images have the best quality, while Before-ET MC resulted in lower quality. For a given motion onset time, image quality increases when correction frequency increases with PMC, RMC, or hybrid MC. With reverse RMC, image quality decreases when the correction frequency is reduced. The same tendencies are seen in the in vivo experiments, except in the case of high amplitude with Before-ET RMC, which resulted in lower quality compared to the uncorrected image.

GRAPPA-related effects

The results of using internal or external acquired GRAPPA reference data for RMC are shown in Figure 8. Quantitative evaluations, in Figure 8A and Figure 8B, do not show a clear difference in SSIM between RMC with integrated versus external ACS acquisition. However, for the continuous motion experiment the RMS discrepancy shows increased motion during the scan with external ACS, which reduced the baseline artifact level in the *uncorrected* external ACS images, as seen from the top row in Figure 8C and the blue “No MC” data points in Figure 8A. Motion parameters for all scans are shown in Supporting Information Figure S 5. Figure 8C and Figure 8D show the reconstructed images corrupted by continuous and discrete motion respectively. Artifacts are evident in RMC images with both integrated and external ACS. Within-ET PMC results in superior image quality compared to Within-ET RMC with either integrated or external ACS in both tested motion patterns.

The results of the comparison of PMC and RMC performed on scans without GRAPPA acceleration (Subject 6) are shown in Figure 9. The quantitative evaluations in Figure 9A and 9B and the reconstructed images in Figure 9C show that both methods lead to improved image quality. However, images corrected by RMC contain notably more motion artifacts compared to images corrected by PMC, although the motion in the PMC scans was higher. The recorded motion parameters are shown in Supporting Information Figure S 6.

Discussion

The experimental results showed that the correction performance of PMC was superior to RMC during the tested discrete and continuous motion patterns. In the presence of continuous motion, increasing the correction frequency of PMC and RMC from no correction to Within-ET updates lead to an improvement in the image quality corresponding with a reduction in the encoding error of the correction. This improvement in image quality with correction frequency was also demonstrated with a hybrid approach that applied additional RMC to data acquired with Before-ET PMC. Experiments without GRAPPA acceleration confirmed that the superior performance of PMC compared to RMC is due to the lack of k-space under-sampling.

Comparison of PMC and RMC

Both PMC and RMC improve the image quality substantially in cases of discrete and periodic continuous motion for the two tested motion amplitudes. PMC resulted in higher image quality than RMC and the improvement in quality increases when the amplitude of the motion is increased, as shown in Figure 4. This is relevant to clinical scans where substantial head movement is expected. It also implies that the performance of PMC and RMC in research scans with compliant subjects is probably similar.

The periodic continuous motion was more challenging to correct retrospectively compared to the discrete motion patterns. For both tested motion amplitudes, RMC provides a reduction in the amount of motion artifacts, especially in the front of the brain (the region that moves the most during head shaking). However, RMC does not fully resolve the signal loss and ghosting as seen in Figure 3.

PMC and RMC have not been directly compared in previous studies. Visual assessment of the results in Zahneisen et al, 2016 [27] shows similar performance of PMC and RMC during a discrete motion pattern, although there was substantial variation in motion amplitude between the PMC and RMC scans.

GRAPPA-related effects

In this study, the majority of the scans were acquired with GRAPPA acceleration, consistent with typical use of parallel imaging to accelerate 3D-encoded MRI, and with integrated ACS data. In our implementation of RMC based on a widely-used toolbox[12], both the estimation of GRAPPA weights and reconstruction of missing data were performed before the motion correction. This is not the case for PMC, where all the data, including the reference data, are motion corrected before the reconstruction. Using external ACS acquisition, to test whether estimation of the GRAPPA weights without intentional motion would improve final image quality, did not show a clear benefit in image quality, and PMC resulted in better image quality than RMC with either integrated or external ACS (Figure 8).

Experiments without GRAPPA (Figure 9) demonstrate that PMC leads to superior image quality, which is similar to the findings of the experiment with GRAPPA (Figures 2, 3, and 8 and Supporting Information Figure S3). This demonstrates that the superior performance of PMC compared to RMC can be attributed to the lack of k-space undersampling violating the Nyquist criterion.

Under-sampled k-space during motion

This study has empirically confirmed the expected disadvantage of RMC for 3D-encoded sequences – that it suffers from k-space under-sampling in the presence of head rotation[8] – showing that there is a measurable image quality improvement with PMC. The repositioning of k-space lines in the RMC method to account for motion causes these Nyquist violations. This effect is seen in the corrected k-space from the scan during large periodic continuous motion in Supporting Information Figure S 4, which shows that the repositioning of the k-space lines during RMC resulted in under-sampled regions close to the center of k-space. Using methods that compensate for the k-space undersampling, such as motion-aware

iterative parallel imaging reconstructions [45], may reduce artifacts in the retrospectively corrected images.

We expect that these results based on sequential Cartesian k-space acquisition will generalize to situations when motion results in contiguous “chunks” of under-sampled k-space. The phase-encode ordering and relative timing of motion (e.g. see Supporting Information Figure S2) are relevant to the extent and location of k-space under-sampling when there is head rotation. Similar comparisons with distributed [18] or radial [17,31] k-space sampling are interesting areas of future work.

Effect of correction frequency on RMC performance

The results of the continuous motion experiments in Figures 5, 6, and 7 show that increasing the correction frequency of RMC and thereby reducing the encoding error substantially improves the image quality. Previous work has shown that increasing the correction frequency of PMC in MPRAGE from no correction, to Before-ET, to Within-ET results in a gradual reduction of motion artifacts [26], and this study shows that the same is true for RMC.

This work also demonstrates that the correction frequency of a Before-ET PMC scan can be retrospectively increased to Within-ET. This hybrid prospective-retrospective MC improves the image quality substantially compared to the quality of the acquired Before-ET PMC images. The quantitative image quality of the HMC is also superior compared to Within-ET RMC from PMC off data. This suggests a hybrid approach with initial Before-ET PMC could ensure that the k-space is roughly uniformly sampled and subsequently RMC could fine-tune the acquired data.

The phantom experiment consisted of three scan sessions, where the performed motion pattern was initiated 0, 1, and 2 minutes into the sequence, respectively. The results in Figure 7A and in Supporting Information Figure S 2 show that motion occurring further into the sequences causes more motion-related artifacts compared to the same motion occurring at the start of the sequence. This confirms that motion affecting the center of k-space is more detrimental to image quality as measured by SSIM.

Tracking noise

Although the results in this work show a superior correction performance of PMC, in general the PMC approach is sensitive to errors and noise from the tracking modality [27,45,46]. RMC can be less sensitive to tracking noise and it preserves the original uncorrected image because the correction takes place after all the data are acquired. Also, more effective temporal filtering of the tracking signal is possible retrospectively. Zahneisen et al. [27] and Maclaren et al. [45] have previously demonstrated that RMC can be used to reduce artifacts caused by tracking noise in a PMC scan. This was done by retrospectively estimating the residual tracking noise through filtering and then using reverse motion correction on the acquired PMC data. The hybrid approach of increasing the update frequency of a Before-ET PMC scan to a Within-ET MC retrospectively is a potential solution to the tracking noise if a Before-ET PMC scan is more robust to tracking noise.

Another synergy combining PMC and RMC is to estimate the uncorrected image through reverse correction as shown in Figures 5 and 6. Reverse correction can be used for 3D-encoded sequences where retrospective correction is not limited by through-slice motion. The possibility of generating the uncorrected image with reverse motion correction [27,40] simplifies the evaluation of PMC especially in a clinical setting where it is not possible to acquire scans with and without PMC during the same motion-pattern. In terms of implementation in the vendor image reconstruction, reverse correction would share the same framework as retrospective motion correction but would use the inverse of the motion transformations that were prospectively applied.

Conclusions

This study has demonstrated that the reduction in local Nyquist violations with prospective motion correction in Cartesian 3D-encoded MPRAGE leads to measurable improvements in image quality compared to retrospective motion correction. Comparisons were performed using the same markerless, high-frequency, optical motion tracking during discrete and continuous motion. In the presence of continuous motion, increasing the correction frequency of prospective and retrospective correction during MPRAGE echo-trains improves image quality. Hybrid correction combining PMC and RMC to retrospectively increase the correction frequency of data acquired with low-frequency Before-ET PMC also resulted in improved image quality.

Supplementary Material

Refer to Web version on PubMed Central for supplementary material.

Acknowledgements

We are grateful for support for this research which was provided in part by the National Institute of Biomedical Imaging and Bioengineering (R21EB029641); National Institute of Child Health and Development (R01HD093578, R01HD099846, R01HD085813); Innovation Fund Denmark (8053-00155B), and was made possible by resources provided by Shared Instrumentation Grants (S10OD025253 and MGH ECOR, 1S10RR023401, 1S10RR019307, and 1S10RR023043)

References

1. Reuter M, Tisdall MD, Qureshi A, Buckner RL, van der Kouwe AJW, Fischl B. Head motion during MRI acquisition reduces gray matter volume and thickness estimates. Neuroimage. 2015;107:107–115. doi:10.1016/j.neuroimage.2014.12.006 [PubMed: 25498430]
2. Tisdall MD, Reuter M, Qureshi A, Buckner RL, Fischl B, van der Kouwe AJW. Prospective motion correction with volumetric navigators (vNavs) reduces the bias and variance in brain morphometry induced by subject motion. Neuroimage. 2016;127:11–22. doi:10.1016/j.neuroimage.2015.11.054 [PubMed: 26654788]
3. Andre JB, Bresnahan BW, Mossa-Basha M, et al. Toward quantifying the prevalence, severity, and cost associated with patient motion during clinical MR examinations. J Am Coll Radiol. 2015;12(7):689–695. doi:10.1016/j.jacr.2015.03.007 [PubMed: 25963225]
4. Sanders RD, Hassell J, Davidson AJ, Robertson NJ, Ma D. Impact of anaesthetics and surgery on neurodevelopment: An update. Br J Anaesth. 2013;110:53–72. doi:10.1093/bja/aet054
5. Blumenthal D, Tavenner M. Anesthesia and Developing Brains — Implications of the FDA Warning. N Engl J Med. 2017;376(10):905–907. doi:10.1056/NEJMpl002530 [PubMed: 28177852]

6. Slipsager JM, Glimberg SL, Søgaard J, et al. Quantifying the Financial Savings of Motion Correction in Brain MRI : A Model-Based Estimate of the Costs Arising From Patient Head Motion and Potential Savings From Implementation of Motion Correction. J Magn Reson Imaging. 2020:1–8. doi:10.1002/jmri.27112
7. Haacke EM, Patrick JL. Reducing motion artifacts in two-dimensional Fourier transform imaging. Magn Reson Imaging. 1986;4(4):359–376. doi:10.1016/0730-725X(86)91046-5 [PubMed: 3669950]
8. Maclaren J, Herbst M, Speck O, Zaitsev M. Prospective Motion Correction in Brain Imaging: A Review. Magn Reson Med. 2013;69(3):621–636. doi:10.1002/mrm.24314 [PubMed: 22570274]
9. Van der Kouwe AJW, Benner T, Dale AM. Real-time rigid body motion correction and shimming using cloverleaf navigators. Magn Reson Med. 2006;56(5):1019–1032. doi:10.1002/mrm.21038 [PubMed: 17029223]
10. White N, Roddey C, Shankaranarayanan A, et al. PROMO: Real-time prospective motion correction in MRI using image-based tracking. Magn Reson Med. 2010;63(1):91–105. doi:10.1002/mrm.22176 [PubMed: 20027635]
11. Tisdall MD, Hess AT, Reuter M, Meintjes EM, Fischl B, van der Kouwe AJW. Volumetric navigators for prospective motion correction and selective reacquisition in neuroanatomical MRI. Magn Reson Med. 2012;68(2):389–399. doi:10.1002/mrm.23228 [PubMed: 22213578]
12. Gallichan D, Marques JP, Gruetter R. Retrospective correction of involuntary microscopic head movement using highly accelerated fat image navigators (3D FatNavs) at 7T. Magn Reson Med. 2016;75(3):1030–1039. doi:10.1002/mrm.25670 [PubMed: 25872755]
13. Wallace TE, Afacan O, Waszak M, Kober T, Warfield SK. Head motion measurement and correction using FID navigators. Magn Reson Med. 2019;81(1):258–274. doi:10.1002/mrm.27381 [PubMed: 30058216]
14. Pipe JG. Motion correction with PROPELLER MRI: application to head motion and free-breathing cardiac imaging. Magn Reson Med. 1999;42(5):963–969. doi:10.1002/(SICI)1522-2594(199911)42:5<963::AID-MRM17>3.0.CO;2-L [PubMed: 10542356]
15. Cordero-Grande L, Teixeira RPAG, Hughes EJ, Hutter J, Price AN, Hajnal JV. Sensitivity Encoding for Aligned Multishot Magnetic Resonance Reconstruction. IEEE Trans Comput Imaging. 2016;2(3):266–280. doi:10.1109/tci.2016.2557069
16. Haskell MW, Cauley SF, Wald LL. TArgeted Motion Estimation and Reduction (TAMER): Data consistency based motion mitigation for mri using a reduced model joint optimization. IEEE Trans Med Imaging. 2018;37(5):1253–1265. doi:10.1109/TMI.2018.2791482 [PubMed: 29727288]
17. Kecskemeti S, Samsonov A, Velikina J, et al. Robust motion correction strategy for structural MRI in unsedated children demonstrated with three-dimensional radial MPnRAGE. Radiology. 2018;289(2):509–516. doi:10.1148/radiol.2018180180 [PubMed: 30063192]
18. Cordero-Grande L, Ferrazzi G, Teixeira RPAG, O'Muircheartaigh J, Price AN, Hajnal JV. Motion-corrected MRI with DISORDER: Distributed and incoherent sample orders for reconstruction deblurring using encoding redundancy. Magn Reson Med. 2020;84(2):713–726. doi:10.1002/mrm.28157
19. Zaitsev M, Dold C, Sakas G, Hennig J, Speck O. Magnetic resonance imaging of freely moving objects: prospective real-time motion correction using an external optical motion tracking system. Neuroimage. 2006;31(3):1038–1050. [PubMed: 16600642]
20. Ooi MB, Krueger S, Thomas WJ, Swaminathan SV, Brown TR. Prospective Real-Time Correction for Arbitrary Head Motion Using Active Markers. Magn Reson Med. 2009;62(4):943–954. doi:10.1002/mrm.22082 [PubMed: 19488989]
21. Aksoy M, Forman C, Straka M, et al. Real-time optical motion correction for diffusion tensor imaging. Magn Reson Med. 2011;66(2):366–378. doi:10.1002/mrm.22787 [PubMed: 21432898]
22. Aranovitch A, Haeberlin M, Gross S, et al. Prospective motion correction with NMR markers using only native sequence elements. Magn Reson Med. 2018;79(4):2046–2056. doi:10.1002/mrm.26877 [PubMed: 28840611]
23. van Niekerk A, van der Kouwe A, Meintjes E. Toward "plug and play" prospective motion correction for MRI by combining observations of the time varying gradient and static vector fields. Magn Reson Med. 2019;82(3):1214–1228. doi:10.1002/mrm.27790 [PubMed: 31066109]

24. Olesen OV, Jørgensen MR, Paulsen RR, Højgaard L, Roed B, Larsen R. Structured Light 3D Tracking System for Measuring Motions in PET Brain Imaging. In: SPIE Medical Imaging. Vol 7625.; 2010:76250X.
25. Slipsager JM, Ellegaard AH, Glimberg SL, et al. Markerless motion tracking and correction for PET, MRI, and simultaneous PET/MRI. PLoS One. 2019;14(4):1–17. doi:10.1371/journal.pone.0215524
26. Frost R, Wighton P, Karahanoğlu FI, et al. Markerless high-frequency prospective motion correction for neuroanatomical MRI. Magn Reson Med. 2019;82(1):126–144. doi:10.1002/mrm.27705 [PubMed: 30821010]
27. Zahneisen B, Keating B, Singh A, Herbst M, Ernst T. Reverse retrospective motion correction. Magn Reson Med. 2016;75(6):2341–2349. doi:10.1002/mrm.25830 [PubMed: 26140504]
28. Atkinson D, Hill DLG, Stoyle PNR, et al. Automatic compensation of motion artifacts in MRI. Magn Reson Med. 1999;41(1):163–170. doi:10.1002/(SICI)1522-2594(199901)41:l<163::AID-MRM23>3.0.CO;2-9 [PubMed: 10025625]
29. Loktyushin A, Nickisch H, Pohmann R, Schölkopf B. Blind retrospective motion correction of MR images. Magn Reson Med. 2013;70(6):1608–1618. doi:10.1002/mrm.24615 [PubMed: 23401078]
30. Norbeck O, van Niekerk A, Avventi E, et al. T1-FLAIR imaging during continuous head motion: Combining PROPELLER with an intelligent marker. Magn Reson Med. 2021;85(2):868–882. doi:10.1002/mrm.28477 [PubMed: 32871026]
31. Polak D, Cauley S, Bilgic B, et al. Scout Acquisition enables rapid Motion Estimation (SAME) for retrospective motion mitigation. In: 28th Annual Meeting of the International Society of Magnetic Resonance in Medicine. ; 2020:Abstract 463.
32. Gretsch F, Mattern H, Gallichan D, Speck O. Fat navigators and Moiré phase tracking comparison for motion estimation and retrospective correction. Magn Reson Med. 2020;83(1):83–93. doi:10.1002/mrm.27908 [PubMed: 31400041]
33. Eschelbach M, Aghaeifar A, Bause J, et al. Comparison of prospective head motion correction with NMR field probes and an optical tracking system. Magn Reson Med. 2019;81(1):719–729. doi:10.1002/mrm.27343 [PubMed: 30058220]
34. Slipsager JM, Glimberg SL, Højgaard L, et al. Comparison of Prospective and Retrospective Motion Correction for 3D Structural Brain MRI. In: 28th Annual Meeting of the International Society of Magnetic Resonance in Medicine. ; 2020:Abstract 0466.
35. Olesen OV, Paulsen RR, Hojgaard L, Roed B, Larsen R. Motion Tracking for Medical Imaging: A Nonvisible Structured Light Tracking Approach. IEEE Trans Med Imaging. 2012;31(1):79–87. doi:10.1109/TMI.2011.2165157 [PubMed: 21859614]
36. Olesen OV, Sullivan JM, Mulnix T, et al. List-Mode PET Motion Correction Using Markerless Head Tracking: Proof-of-Concept With Acans of Human Subject. IEEE Trans Med Imaging. 2013;32(2):200–209. doi:10.U09/TMI.2012.2219693 [PubMed: 23008249]
37. RetroMoCoBox Toolbox. https://github.com/dgallichan/retroMoCoBox.
38. Griswold MA, Jakob PM, Heidemann RM, et al. Generalized Autocalibrating Partially Parallel Acquisitions (GRAPPA). Magn Reson Med. 2002;47(6):1202–1210. doi:10.1002/mrm.10171 [PubMed: 12111967]
39. Schwarzl A, Knoll F. Implementation of Non Uniform Fast Fourier Transformation. https://github.com/andyschwarzl/gpuNUFFT.
40. Frost R, Tisdall MD, Hoffmann M, Fischl B, Salat D, van der Kouwe AJW. Scan-specific assessment of vNav motion artifact mitigation in the HCP Aging study using reverse motion correction. In: 28th Annual Meeting of the International Society of Magnetic Resonance in Medicine. ; 2020:Abstract 467.
41. Jenkinson M Measuring Transformation Error by RMS Deviation. Oxford; 1999.
42. Yoo TS, Ackerman MJ, Lorensen WE, et al. Engineering and Algorithm Design for an Image Processing API: A Technical Report on ITK - The Insight Toolkit. In Proc. of Medicine Meets Virtual Reality,. Westwood J, ed, IOS Press Amsterdam. 2002;85:586–592.
43. Mccormick M, Liu X, Jomier J, Marion C, Ibanez L. Itk: Enabling reproducible research and open science. Front Neuroinform. 2014;8(FEB):1–11. doi:10.3389/fninf.2014.00013 [PubMed: 24501593]

44. Wang Z, Bovik AC, Sheikh HR, Simoncelli EP. Image quality assessment: From error visibility to structural similarity. IEEE Trans Image Process. 2004;13(4):600–612. doi:10.1109/TIP.2003.819861 [PubMed: 15376593]

45. MacLaren J, Lee KJ, Luengviriya C, Speck O, Zaitsev M. Combined prospective and retrospective motion correction to relax navigator requirements. Magn Reson Med. 2011;65(6):1724–1732. doi:10.1002/mrm.22754 [PubMed: 21590805]

46. Singh A, Zahneisen B, Keating B, et al. Optical tracking with two markers for robust prospective motion correction for brain imaging. Magn Reson Mater Physics, Biol Med. 2015;28(6):523–534. doi:10.1007/s10334-015-0493-4

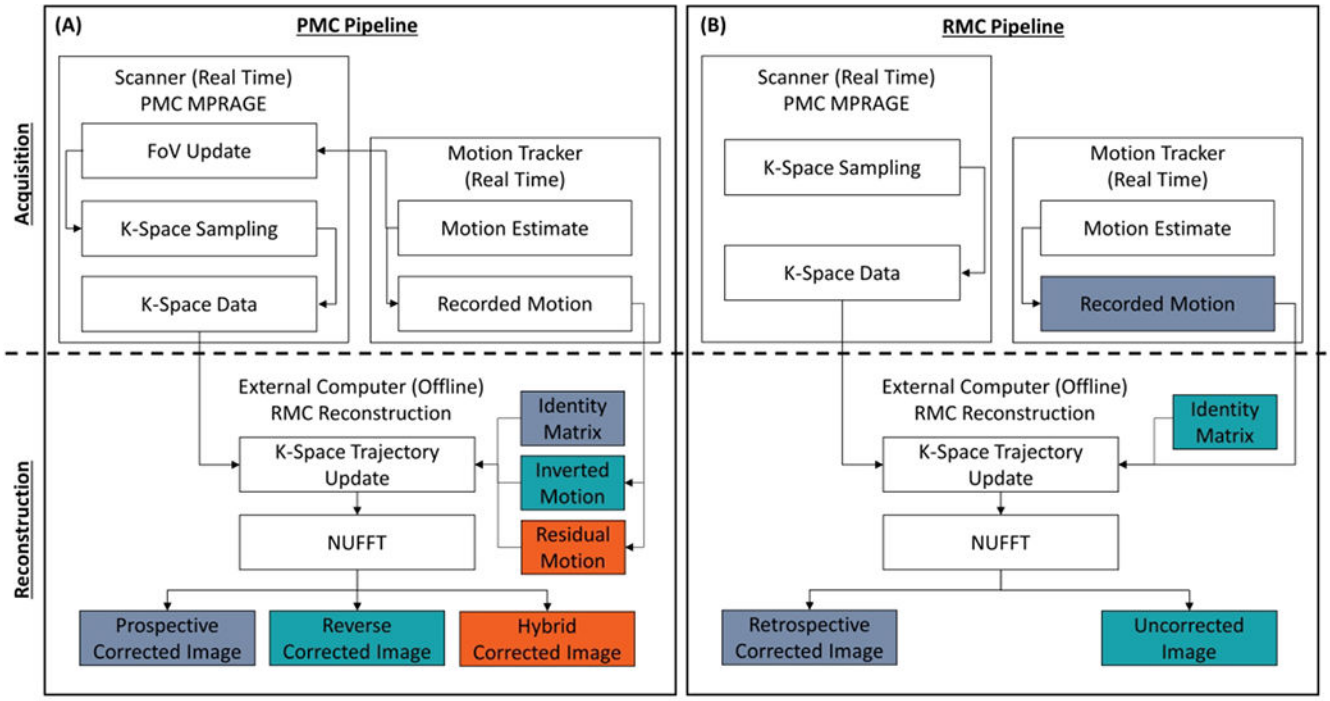

Figure 1.

Flow chart showing the data acquisition and reconstruction pipeline used to generate images without motion correction (MC), with prospective MC (PMC), retrospective MC (RMC), reverse MC, and hybrid PMC and RMC. Matching colors illustrate what type of motion a given image was corrected by. The non-uniform fast Fourier transform (NUFFT) was used to reconstruct the images in all cases. (A) Shows the pipeline for PMC data. The PMC takes place on the scanner, where the field of view (FOV) is updated. The hybrid and the reverse correction were performed during the reconstruction on an external computer. (B) Shows the pipeline for both RMC and without MC. The trajectory of the acquired k-space data was updated with the recorded motion and with the identity matrix to generate the RMC and uncorrected images, respectively.

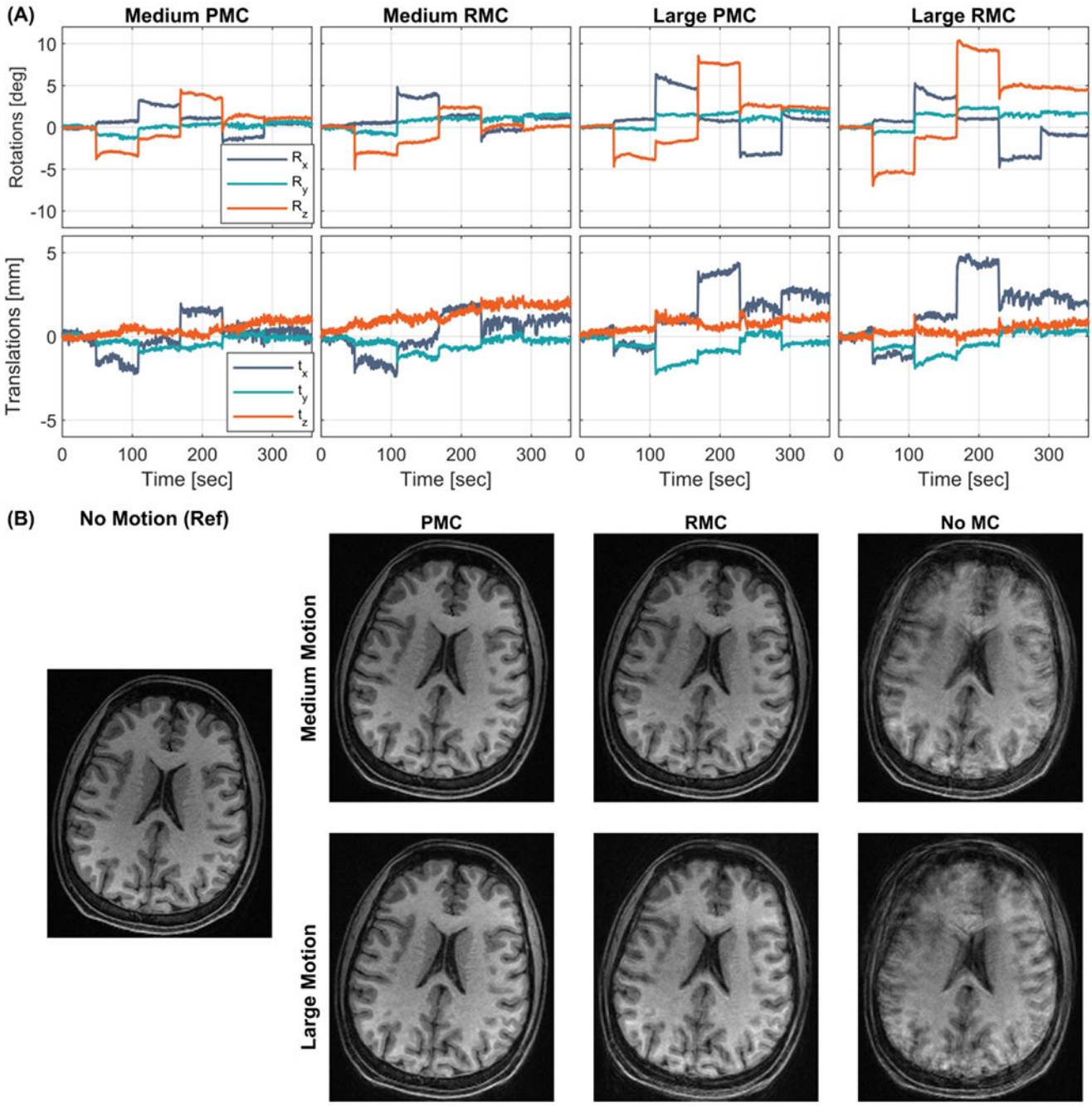

Figure 2.

In vivo comparison of within echo train (Within-ET) PMC, Within-ET RMC, and no MC during scans with discrete motion with medium and large amplitude (Subject 1). (A) The motion measurements during the four scans. (B) MPRAGE image reconstructions from scans with medium and large motion with PMC, RMC, and no correction. The leftmost MPRAGE image was acquired in a scan with no motion and without motion correction and was used as a reference for image quality. PMC: prospective motion correction; RMC retrospective motion correction; no MC: without motion correction.

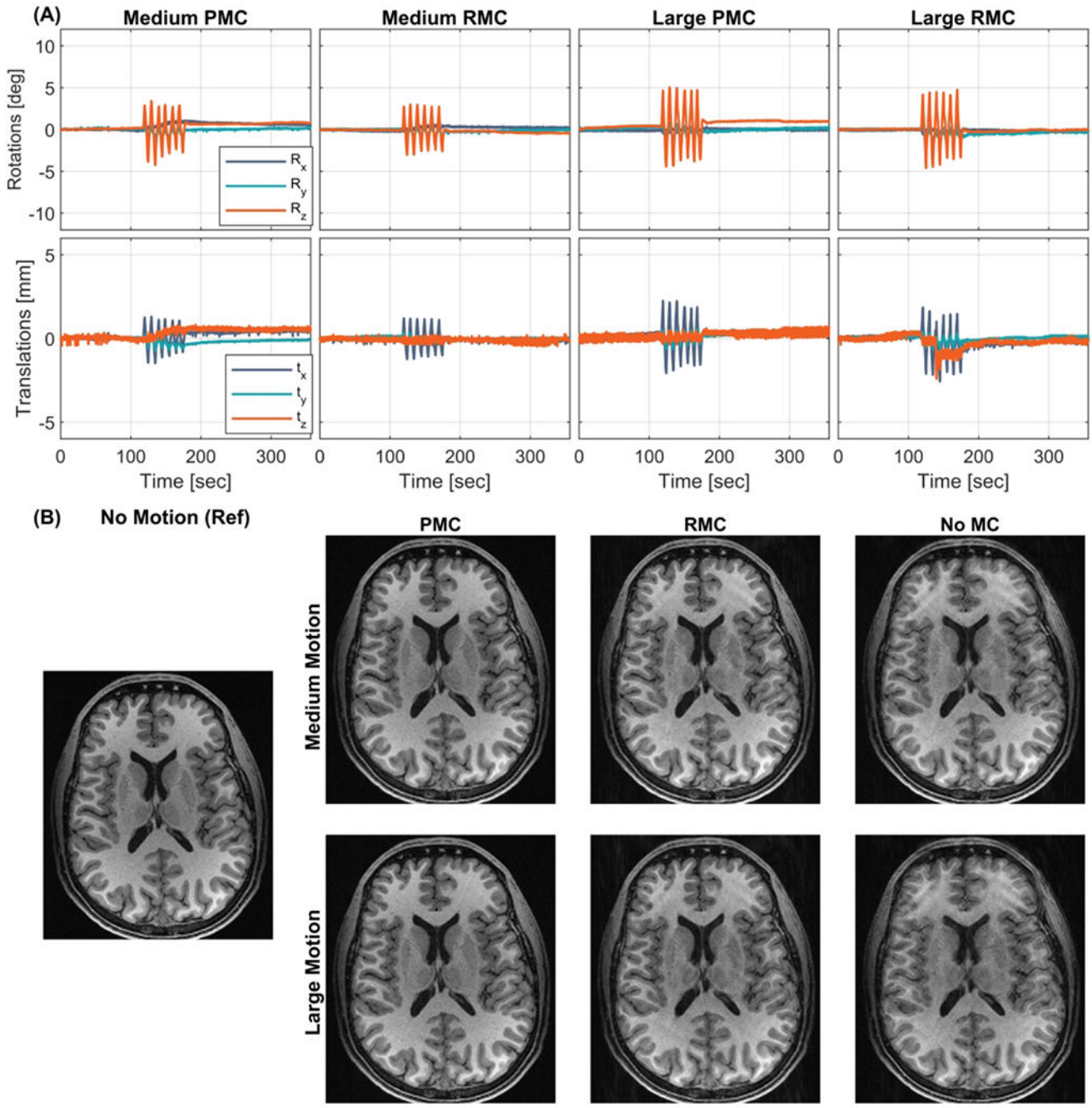

Figure 3.

In vivo comparison of within echo train (Within-ET) PMC, Within-ET RMC, and no MC during periodic continuous motion with medium and large amplitude (Subject 2). (A) The motion measurements during the four scans. (B) MPRAGE image reconstructions from scans with medium and large motion, with PMC, RMC, and no correction. The leftmost MPRAGE image was acquired in a scan with no motion and without motion correction and was used as a reference for image quality. PMC: prospective motion correction; RMC retrospective motion correction; no MC: without motion correction.

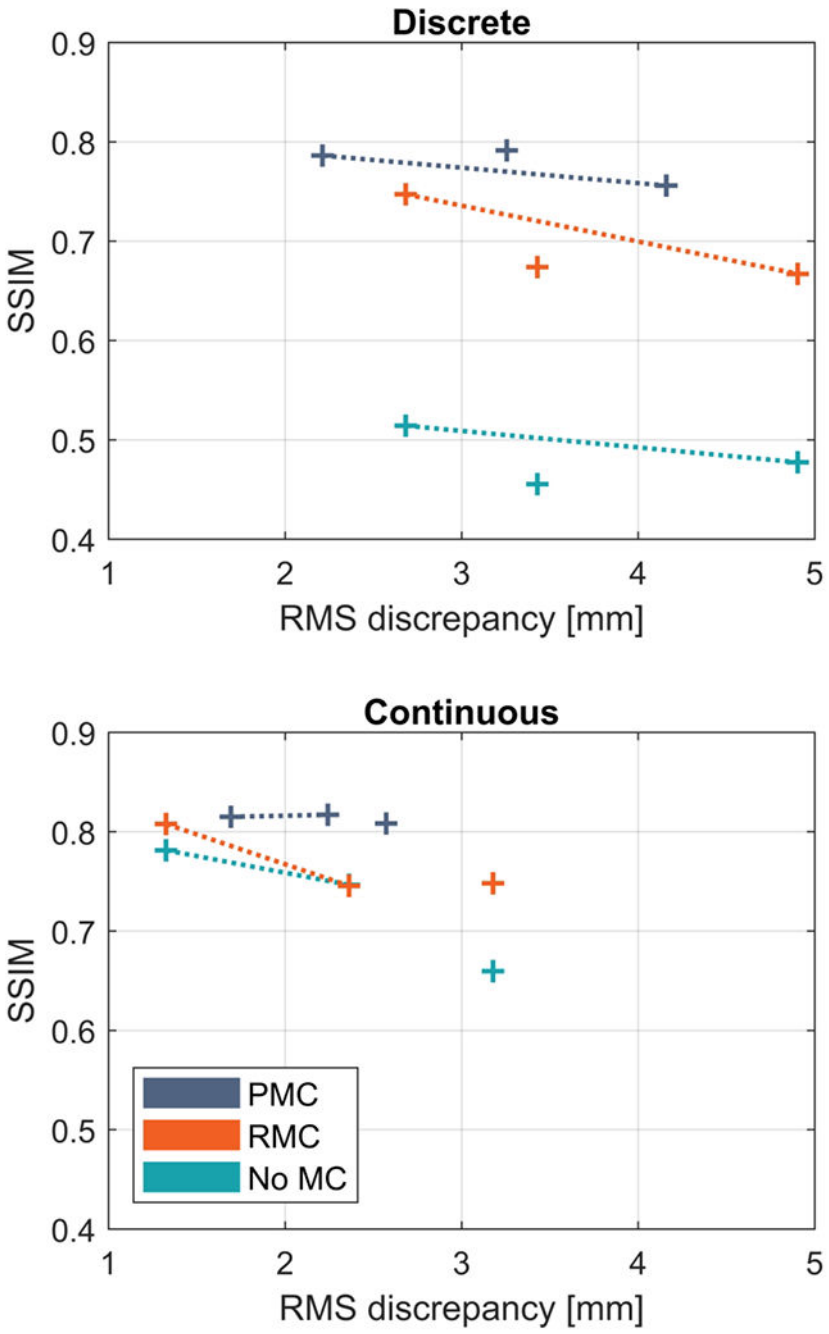

Figure 4.

Quantitative comparison of the correction performance of within echo train (Within-ET) PMC and Within-ET RMC during discrete and continuous motion. The structural similarity index measure (SSIM) relative to a scan without motion correction and intentional motion is plotted as a function of RMS discrepancy between the recorded motion and no motion (identity matrix). Connected points correspond to experiments with the same motion correction but with varied amplitude of motion. PMC: prospective motion correction; RMC retrospective motion correction; no MC: without motion correction.

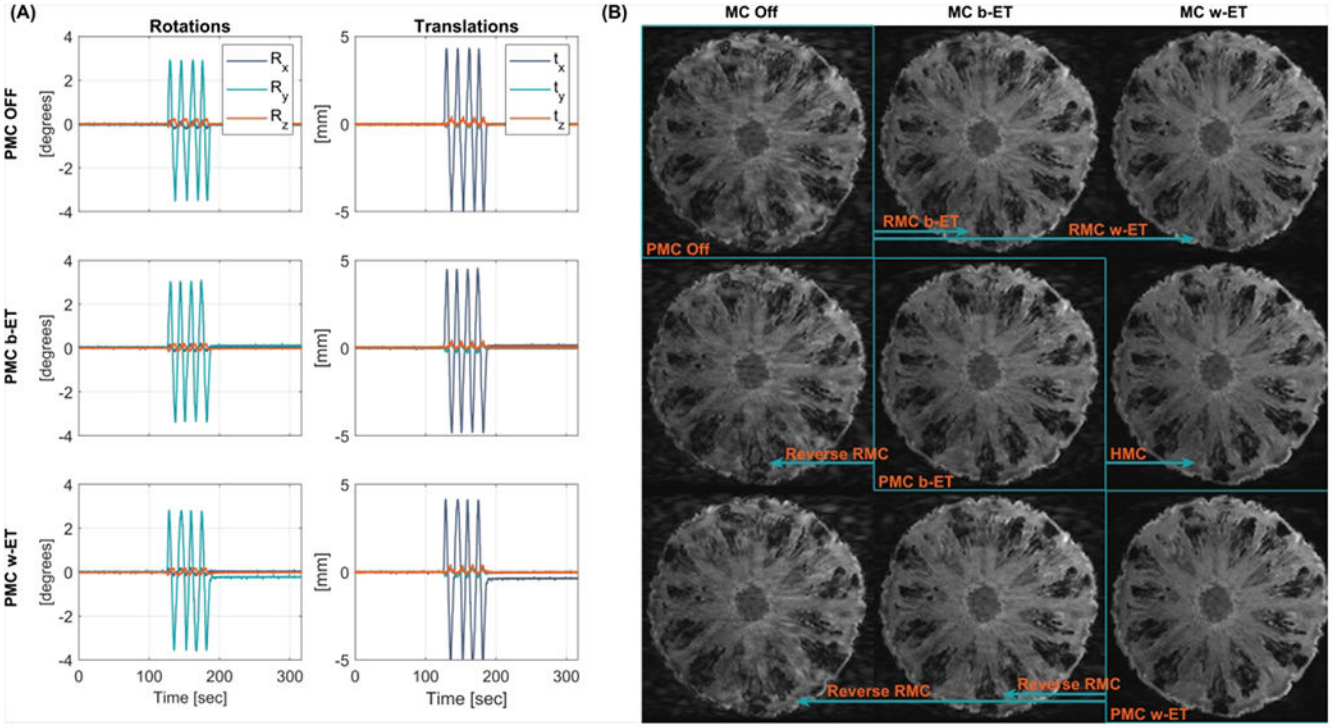

Figure 5.

Phantom comparison of MC OFF, PMC, and RMC during periodic continuous motion. (A) Recorded motion parameters of the performed motion with start time 2 minutes into the sequence. (B) MPRAGE images along the diagonal show increasing image quality and were acquired with PMC off, Before echo train PMC (PMC b-ET), and Within echo train PMC (PMC w-ET). Images outside the diagonal are retrospectively corrected or reverse corrected versions of the highlighted image along the same row (indicated by the arrows). These images include RMC, reverse RMC, and HMC. PMC: prospective motion correction; RMC retrospective motion correction; MC OFF: without motion correction; HMC: hybrid prospective, retrospective motion correction.

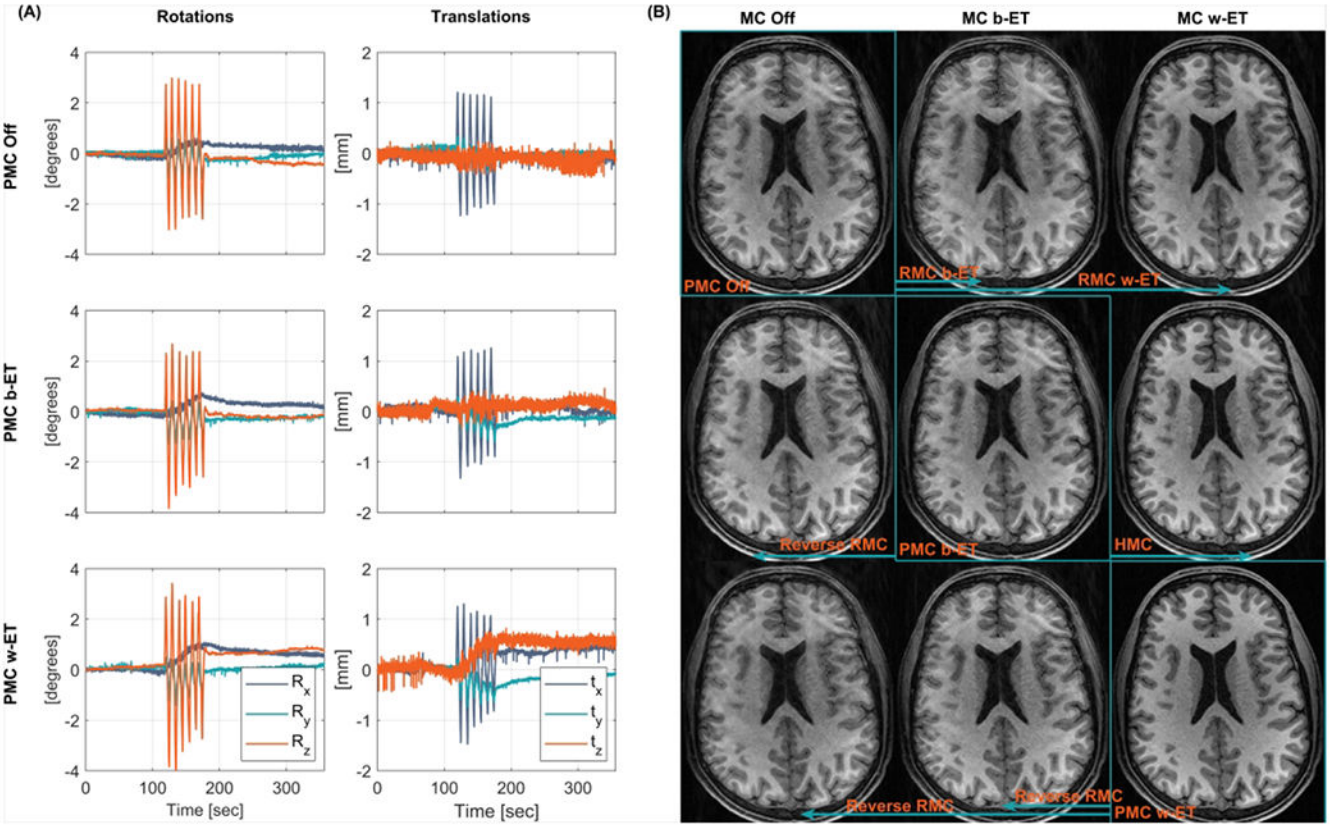

Figure 6.

In vivo comparison of MC OFF, PMC, and RMC during periodic continuous motion (large amplitude, subject 2. (A) Recorded motion parameters of the performed motion. (B) MPRAGE images along the diagonal were acquired with PMC off, Before echo train PMC (PMC b-ET), and Within echo train PMC (PMC w-ET). Images outside the diagonal are retrospectively corrected or reverse corrected versions of the highlighted image along the same row (indicated by the arrows). These images include RMC, reverse RMC, and HMC. PMC: prospective motion correction; RMC retrospective motion correction; MC OFF: without motion correction; HMC: hybrid prospective, retrospective motion correction.

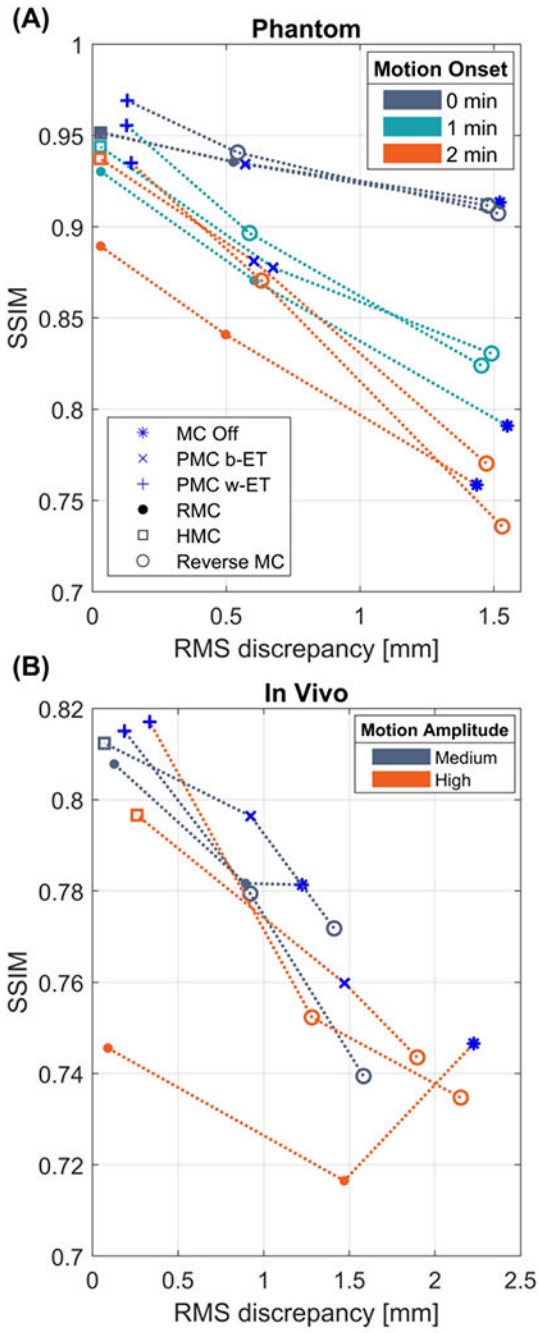

Figure 7.

Structural similarity index measure (SSIM) as a function of RMS discrepancy between true motion and encoded motion. Blue markers correspond to data acquired with PMC off, b-ET PMC, and w-ET PMC. Connected points represent images reconstructed from the same data. The color corresponds to a given type of motion. In the phantom scans (A) the colors correspond to the motion starting 0, 1, and 2 minutes into the sequences. In the in vivo scans (B) the colors correspond to the medium and high motion amplitude experiments. The MC off images in (A) show that motion occurring further into the sequences (closer to the

k-space center) is more disruptive of the image quality. Both figures show that increasing the correction frequency from Before-ET to Within-ET results in lower RMS-discrepancy and higher image quality. PMC: prospective motion correction; RMC retrospective motion correction; MC OFF: without motion correction; HMC: hybrid prospective, retrospective motion correction; b-ET: before echo train; w-ET within echo train.

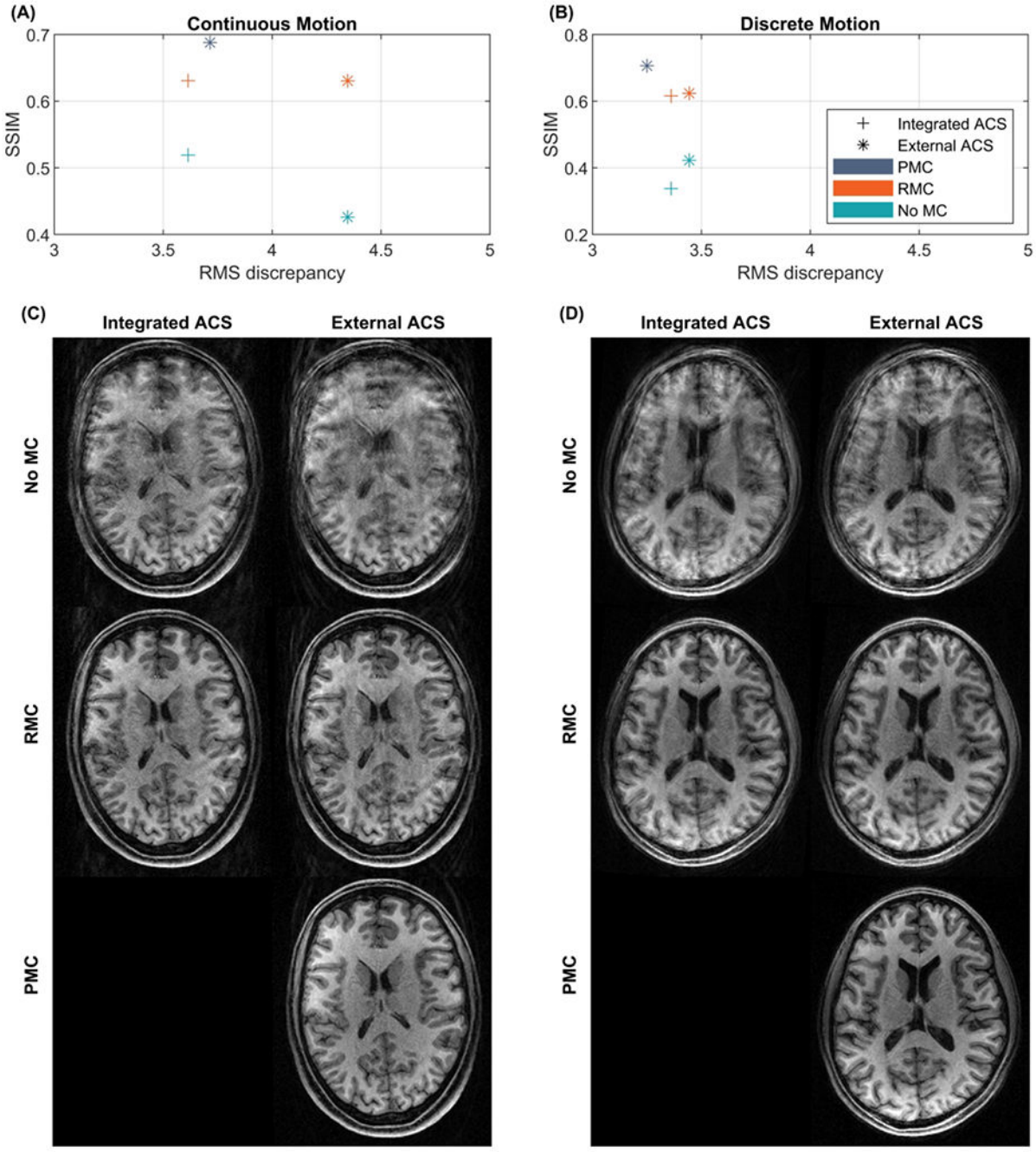

Figure 8.

Comparison of image quality of MPRAGE scans with integrated or externally acquired GRAPPA ACS data. Quantitative comparisons are shown in (A) and (B), where the structural similarity index measure (SSIM) relative to a scan without intentional motion and with external reference and no MC is plotted as a function of the root mean square (RMS) discrepancy. (C) reconstructed images corrupted by continuous motion. (D) Reconstructed images corrupted by discrete motion. PMC: prospective motion correction;

RMC retrospective motion correction; No MC: without motion correction; ACS: auto-calibration signal.

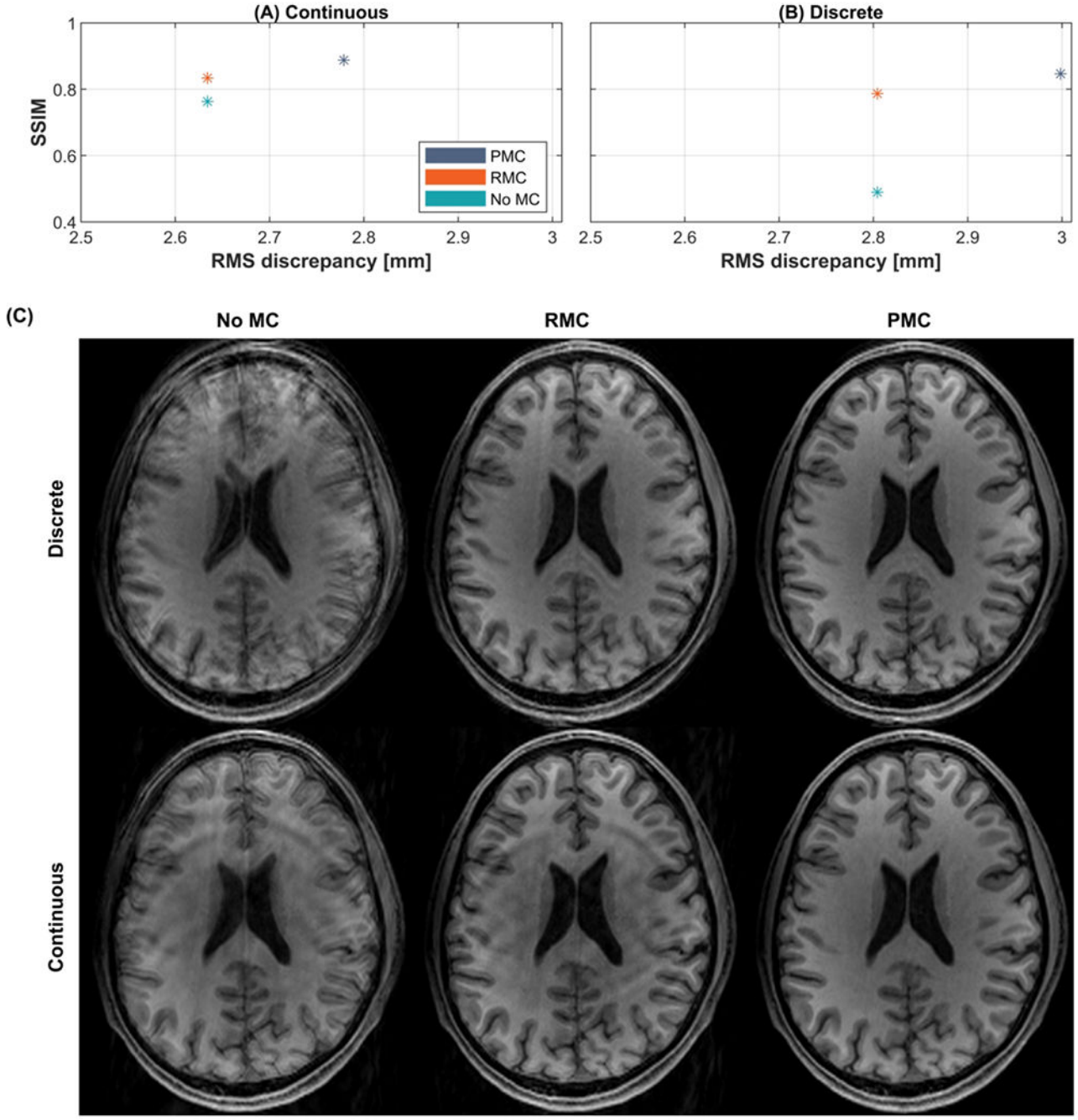

Figure 9.

Comparison of image quality of MPRAGE scans without GRAPPA. Quantitative comparisons are shown in (A) and (B), where the structural similarity index measure (SSIM) relative to a scan without motion correction and intentional motion with no MC is plotted as a function of the root mean square (RMS) discrepancy. (C) Reconstructed images corrupted by discrete or continuous motion. PMC: prospective motion correction; RMC retrospective motion correction; No MC: without motion correction; ACS: auto-calibration signal.

Table 1

List of the performed experiments.

Session	Motion pattern	Experiments	Performed sequences
Phantom	Continuous	3 experiments were performed, where the motion period began 0, 1, and 2 minutes into the sequence.	3 x no MC 3 x Before-ET-PMC 3 x Within-ET-PMC
Subject 1	Discrete	The pattern was performed with medium and high motion amplitude.	2 x no MC 2 x Within-ET-PMC
Subject 2	Continuous	The pattern was performed with medium and high motion amplitude.	2 x no MC 2 x Before-ET-PMC 2 x Within-ET-PMC
Subject 3	Discrete Continuous	Both the discrete and the continuous motion patterns were performed	2 x no MC 2 x Within-ET-PMC
Subject 4	Discrete	The pattern was repeated in all 3 scans	1 x no MC, External ACS 1 x no MC, Integrated ACS 1 x Within-ET-PMC, External ACS
Subject 5	Continuous	The pattern was repeated in all 3 scans	1 x no MC, External ACS 1 x no MC, Integrated ACS 1 x Within-ET-PMC, External ACS
Subject 6	Discrete Continuous	Both the discrete and the continuous motion patterns were performed	2 x no MC, No GRAPPA 2 x Within-ET-PMC, No GRAPPA